Comparison of slant-path scintillometry, sonic anemometry and high-speed videography for vertical profiling of turbulence in the atmospheric surface layer

Derek J Griffith*[a], Detlev Sprung[b], Erik Sucher[b], Arshath Ramkilowan[a], Lufuno Vhengani[a]
[a]Optronic Sensor Systems (OSS), Council for Scientific and Industrial Research (CSIR),
P O Box 395, Pretoria 0001, South Africa
[b]Fraunhofer Institute of Optronics, System Technologies and Image Exploitation (IOSB),
Gutleuthausstraße 1, 76275 Ettlingen, Germany

ABSTRACT

The optical effect of atmospheric turbulence greatly inhibits the achievable range of Detection, Recognition and Identification (DRI) of targets when using imaging sensors within the surface layer. Since turbulence tends to be worst near the ground and decays with height, the question often arises as to how much DRI range could be gained by elevating the sensor. Because this potential DRI gain depends on the rate of decay of turbulence strength with height in any particular environment, there is a need to measure the strength profile of turbulence with respect to height in various environments under different atmospheric and meteorological conditions. Various techniques exist to measure turbulence strength, including scintillometry, sonic anemometry, Sound Detection and Ranging (SODAR) and the analysis of point source imagery. These techniques vary in absolute sensitivity, sensitivity to range profile, temporal and spatial response, making comparison and interpretation challenging.

We describe a field experiment using multiple scintillometers, sonic anemometers and point source videography to collect statistics on atmospheric turbulence strength at different heights above ground. The environment is a relatively flat, temperate to sub-tropical grassland area on the interior plateau of Southern Africa near Pretoria. The site in question, Rietvlei Nature Reserve, offers good spatial homogeneity over a substantial area and low average wind speed. Rietvlei was therefore chosen to simplify comparison of techniques as well as to obtain representative turbulence profile data for temperate grassland. A key element of the experimental layout is to place a sonic anemometer 15 m above ground at the centre of a 1 km slant-path extending from ground level to a height of 30 m. An optical scintillometer is operated along the slant-path. The experiment layout and practical implementation are described in detail and initial results are presented.

Keywords: Atmospheric turbulence, sonic anemometer, scintillometer

1. INTRODUCTION

Atmospheric turbulence is very often the factor limiting the achievable range of surveillance tasks using imaging sensors in the atmospheric boundary layer. The vertical profile of turbulence strength in various environments and under different meteorological conditions is therefore important when performing analysis or design of long-range imaging surveillance systems. In most such instances the surveillance sightline is a slant path or passes over undulating terrain. Methods of reducing the impact of turbulence on image quality have strategic value and vertical turbulence profiling can contribute to the development of such methods.

There have been quite a number of published campaigns, executed in various environments, to measure diurnal turbulence strength on horizontal sightlines at fixed height above the surface.[1,2] Likewise, particularly in the astronomy community, there have been many campaigns to measure the vertical turbulence profile of the entire atmosphere. Fewer campaigns have set out to measure the vertical profile with emphasis on the boundary and surface layers. The VerTurM experiment in northern Germany[3] is one of the most comprehensive, long-term efforts to perform this type of measurement. In the campaign described here, measurements were performed using slant-path and horizontal scintillometry, high speed videography of quasi-point-sources and sonic anemometry, with the specific intention of comparing these three measurement techniques. A further goal was to obtain surface layer turbulence strength data representative of a sub-tropical grassland environment.

*dgriffith@csir.co.za; phone +27 12 841 3371; fax +27 12 841 4015; www.csir.co.za

Remote Sensing of Clouds and the Atmosphere XVIII; and Optics in Atmospheric Propagation and Adaptive Systems XVI, edited by Adolfo Comeron, et. al., Proc. of SPIE Vol. 8890, 889014
 · doi: 10.1117/12.2032674

2. METHODS OF TURBULENCE MEASUREMENT

There are a number of techniques to measure turbulence strength, including optical scintillometry, sonic anemometry, rapid thermometry, analysis of point-source imagery, Sound Detection and Ranging (SODAR) along with SODAR Radio-Acoustic Sounding Systems (RASS[3]), Scintillation Detection and Ranging (SCIDAR[4]), Slope Detection and Ranging (SLODAR[5]) and Light Detection and Ranging (LIDAR[6]). These techniques rely on different physical aspects of turbulence and some execute essentially a point measurement, some perform spatial averaging over an optical sightline, while others can resolve turbulence strength as a function of distance along the sightline. These various techniques also have different spatial and temporal response and sensitivity to the underlying turbulence phenomenon, making it challenging to compare results derived from the associated instruments. Data processing to yield turbulence strength sometimes involves underlying assumptions (such as Kolmogorov statistics) which may make inter-comparison difficult or invalid under some circumstances.

2.1 Scintillometry

Scintillometry involves the measurement of the intensity fluctuations of a light source observed over a sightline traversing a turbulent medium. Processing and analysis of the intensity statistics reveals information about the turbulence strength along the path. Intensity fluctuations are caused by turbulence along the full length of the sightline, but most sensitive to turbulence near the centre of the sightline. Two models of Scintec® scintillometers were used in this campaign, namely the SLS20 surface layer laser scintillometer and the BLS900 boundary layer scintillometer. The SLS20 instrument was deployed on a horizontal path 1.7 m above ground level on a flat 100 m transect. Two BLS900 scintillometers were deployed on 1 km slant paths from a mast on which the transmitters (light sources) were mounted at different heights above ground, to two receivers that were both 1.7 m above ground level.

These instruments operate by means of measuring the intensity fluctuations along two slightly separated optical paths and deriving the turbulence strength from the log-amplitude variance and covariance of these fluctuations. Two adjacent paths are used in order to help eliminate the effect of absorption or scatter from aerosols in the path, which varies slowly compared to turbulence. The SLS and BLS instruments have different spatial response to turbulent eddies, mainly due to the different aperture/beam diameters. The SLS20 has source and detector separation of 2.7 mm and a detector diameter of 2.5 mm. The BLS900 has a source diameter (D_t) of 150 mm and receiver diameter (D_r) of 145 mm. The SLS and BLS scintillometers are used over different pathlength magnitudes because the SLS instrument is much more sensitive to turbulence for this reason. The other chief difference between the SLS and BLS instruments is that the BLS version is generally insensitive to inner scale (l_0 which is the smallest spatial scale of refractive index, density or temperature fluctuations) effects, while the SLS version, because of the much narrower laser beam, does respond to the inner scale. Hence, inner scale effects could contribute to discrepancies in results from the two types of instrument, depending on how they are used. The SLS instrument should preferably not be used in situations with varying turbulence strength or spatial spectrum along the sightline (e.g. slant or vertical paths).

The response of the BLS900 to turbulent features at different spatial scales, together with the variation of weighting along the sightline are plotted in Figure 1.[7] The path weighting function of the SLS instrument depends on l_0, but since this instrument was deployed on a horizontal path, the path weighting factor is not important on the assumption that the turbulence is homogenous along the path. Neither instrument has notable response to the outer scale (L_0 which the largest spatial scale of turbulence, generally on the order of metres) and for the purposes of small aperture imaging within the boundary layer, L_0 is of lesser interest.

Since the BLS scintillometers were operated on slant paths, the derived refractive index structure function parameter (C_n^2) is not always the best result to work with. Instead one can work directly with the log-amplitude variances (B_{11} and B_{22}) and the log-amplitude covariance (B_{12}), where the subscripts denote the two slightly separated optical paths referred to above. These more basic measurements are available from both SLS and BLS instruments.

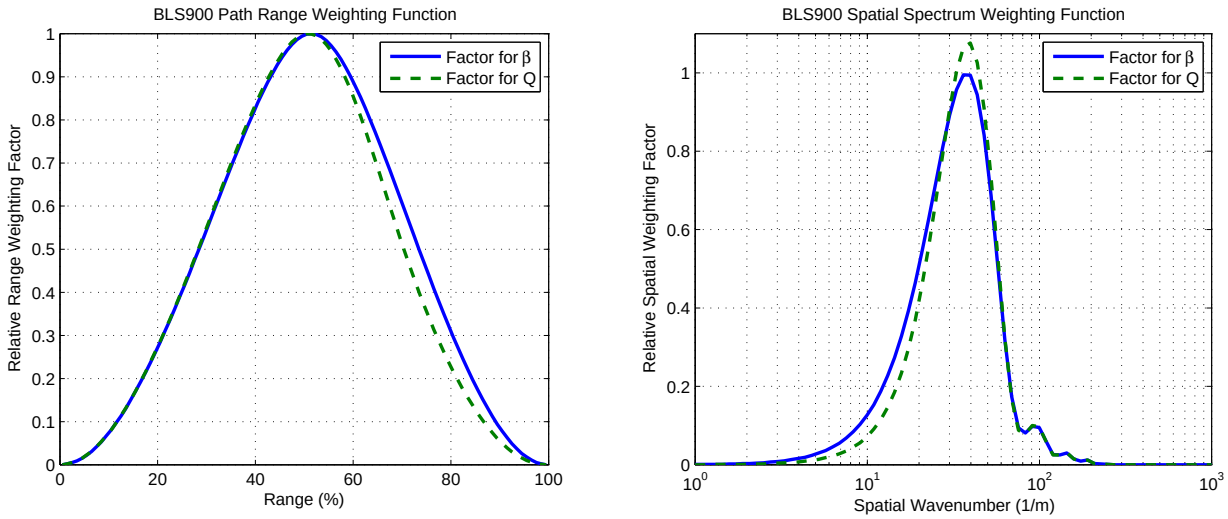

Figure 1. BLS900 Path (left) and Spatial (right) Weighting Functions

Both BLS900 scintillometers used in this campaign were operated at 25 Hz pulse repetition rate rather than the maximum of 125 Hz in order to conserve battery power. This has implications for the reliability of cross-wind measurements, but otherwise should not impact turbulence strength measurements.

2.2 Sonic Anemometry

Sonic anemometers function on the principle that the Speed of Sound (SoS) in a gas varies with the composition and thermodynamic state in a known way. Sonic anemometers that can resolve air flow velocity in all three spatial dimensions use the time-of-flight of sonic pulses transmitted from one of three sound transducers and received at one of another three sound transducers arranged in a suitable spatial configuration. If measurements are repeated at sufficiently high repetition rate, SoS variations due to turbulence can be resolved. Since the pressure and composition of air changes little on the relevant spatial scale, the SoS variations can be attributed largely to temperature fluctuations, which are directly related to variations in refractive index. The thermodynamic state must be measured independently in order to derive the absolute strength of temperature fluctuations (C_T^2).

Three Gill HS-50 research sonic anemometers were deployed on a 15 m mast at the centre of the measurement transect to obtain essentially point measurements of turbulence strength at three heights above ground. The installation of one of the anemometers on the 15 m mast is shown in Figure 4. The temperature and humidity state are measured at the heights of each sonic anemometer (seen attached directly to the mast in Figure 4). The Gill HS-50 has an SoS sample path length of 146 mm, which is on the order of the source size of the BLS900, which is 150 mm in diameter.

2.3 Point Source Videography

This technique makes use of small, high intensity, light sources that are recorded through the atmosphere using a framing video camera. If the camera has sufficiently high frame rate, the time evolution of the turbulence phenomena can be fully resolved. Lower frame rates can be used for statistical work. The video camera used at Rietvlei was a Redlake® MotionPro high speed digital imaging system. The maximum spatial resolution of this camera is 1280×1024 pixels, 12 µm square in size. The maximum frame rate of the camera is dependent on the selected window size. Most video sequences at Rietvlei were recorded with a Nikon® 400 mm focal length f/2.8 lens. The entrance pupil diameter is 143 mm fully open. One camera pixel in object space is about 30 µrad (6.2 arcsec), and projected at 1000 m range was ~30 mm. The total linear Field Of View (FOV) of the camera at 1000 m in the 1280 pixel (long) axis was ~38 m.

The turbulence strength in the sightline from source to camera can be estimated in several ways. Intensity fluctuations in the recorded Point Spread Function (PSF) can be used to obtain a scintillation index. Variations in the position of the PSF can be used to compute the Angle of Arrival (AoA) fluctuations. Most video sequences were recorded at best focus, but some were recorded with a deliberate defocus. Defocusing the lens has the advantage that the image patch is spread over

many more pixels than in the focused mode. This makes it possible to fully open the lens aperture and therefore obtain more signal. If the PSF covers only a few pixels, the derived AoA or scintillation measurements are possibly more susceptible to variations in pixel sensitivity or dark current. Dark signal video sequences were captured at the same exposure times that were used for the point source video sequences in order to be able to subtract the dark signal.

Two types of light sources were used, the first comprising an LED array and the second a quartz halogen lamp with ⌀111 mm reflector (Osram HALOSPOT®). Video sequences of the halogen lamps with narrow spectral filters at various central wavelengths were recorded as well as sequences without spectral filter.

The LED array lamps each comprised seven Luxeon Rebel® Blue ES devices at a central wavelength of 460 nm and spectral full width at half maximum of 20 nm, with a Polymer Optics® hexagonal cluster collimator having 12° total beam angle. The effective diameter of these LED sources was 35.8 mm. The sources were switched on and off by radio remote control. In retrospect, a better means of removing background from the video sequences, including any dark signal, would have been to switch the LEDs on shortly after the start of video capture and perhaps also switch them off near the end of video capture.

The camera was mounted on a sturdy tripod to help reduce any vibrational contribution to the AoA results.

3. EXPERIMENTAL LAYOUT

The instruments comprised a weather station including short and longwave radiometers and soil temperature probes, three scintillometers, a high speed video camera and light sources mounted on masts at two locations. A 15 m pneumatic mast was placed around 500 m downrange from the receivers and a 30 m lattice mast was erected near 1 km downrange. A schematic plan view of the experimental layout is provided in Figure 2.

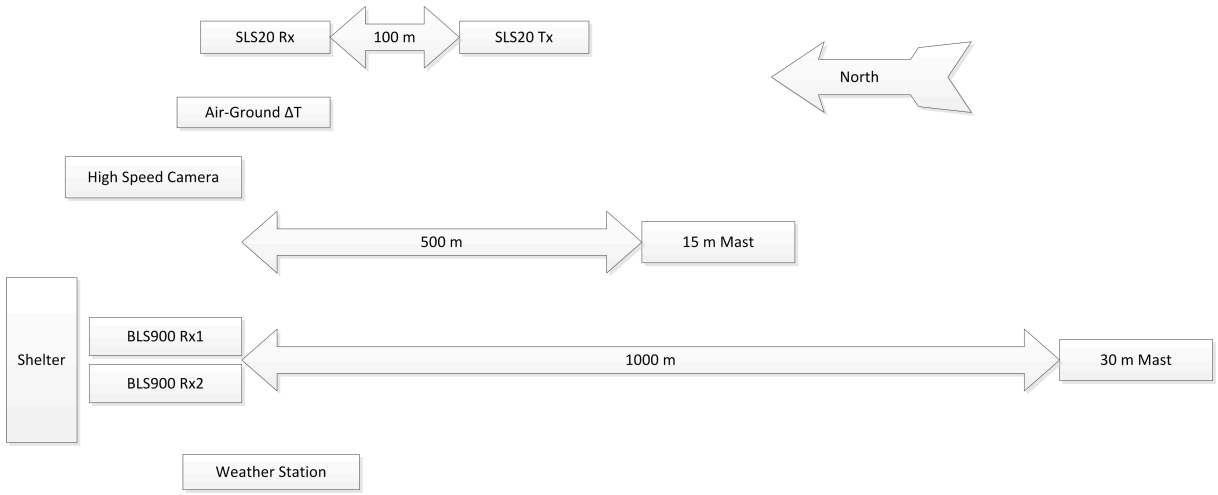

Figure 2. Schematic Plan View of Experimental Layout

A schematic elevation view of the experimental layout is provided in Figure 3. Light sources, including both Light Emitting Diode (LED) arrays and halogen lamps were placed at various heights on the 30 m mast. Three scintillometers were deployed. A Scintec SLS20 was placed at ground level to get a reference turbulence strength measurement at a height of 1.7 m above ground over a distance of 100 m. Two Scintec BLS900 scintillometer receivers were used in conjunction with transmitters near ground level and also near the top of the 30 m mast. Three Gill HS-50 sonic anemometers were positioned at three heights on the 15 m mast. An important element of the layout was that the centre of the sightline from one of the BLS900 receivers to the Tx at the top of the 30 m mast was nearly coincident with the location of the upper sonic anemometer on the 15 m mast.

It was verified by experiment that the two BLS900 transmitters did not create interference at the receivers.

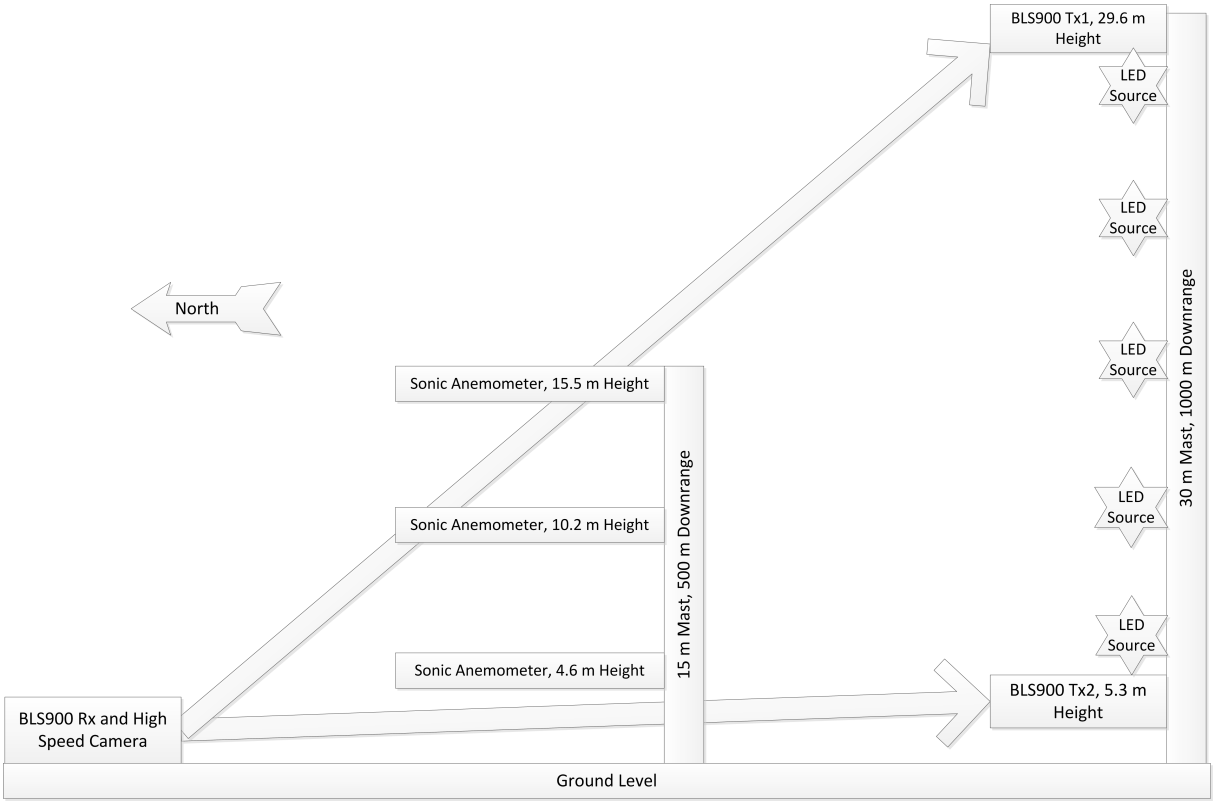

Figure 3. Schematic Elevation View of Experimental Layout

The measurement instruments, location and heights above ground are given in Table 1.

Table 1. Measurement Instruments and Locations

Instrument/Item	Location	Height Above Ground (m)
Scintec BLS900 Receivers (Rx, 2 Units)	Shelter (north end of transect)	1.7 and 1.8
Scintec BLS900 Transmitters (Tx, 2 Units)	30 m Mast (south end of transect)	5.3 and 29.6
Scintec SLS20 Receiver (Rx)	SE of Shelter	1.7
Scintec SLS20 Transmitter (Tx)	100 m South of Rx	1.7
Gill HS-50 Sonic Anemometer (3 Units)	15 m Mast (centre of transect)	4.6; 10.2 and 15.5
Redlake High Speed Camera	Shelter (north end of transect)	1.7
Air-Ground ΔT	SE of Shelter	Ground Level and 1.7
Humidity	Weather Station SW of Shelter	1.9
Air Temperature	Weather Station SW of Shelter	1.9
Visibility	Weather Station SW of Shelter	1.7
Direct and Diffuse Solar Irradiance	Weather Station SW of Shelter	1.9
Down/Upwelling Longwave Irradiance	Weather Station SW of Shelter	1.9
Wind Speed and Direction	Weather Station SW of Shelter	1.9
Blue LED Lamps (5 Units)	30 m Mast (south end of transect)	5.6; 11.6; 17.5; 23.9 and 28.9
HALOSPOT Halogen Lamps (3 Units)	30 m Mast (south end of transect)	2.2; 17.1 and 28.5

In addition to the light sources and instruments listed in Table 1, resolution targets including a Siemens star and 3-bar USAF 1951 targets, were positioned at both the 15 m mast and 30 m mast locations. High speed videography of the resolution targets as well as the light sources on the 30 m mast was recorded. A photograph of the masts, looking in the downrange (southerly) direction from the location of the BLS900 receivers is shown in Figure 4.

Figure 4. Downrange Photograph of Masts (left) and Sonic Anemometer

4. EXPERIMENTAL ENVIRONMENT AND CONDITIONS

The location chosen for the experiment was an area of open, relatively flat, rehabilitated grassland in the Rietvlei Nature Reserve near Pretoria, South Africa. This location was chosen on the basis of a number of criteria including the open and uniform fetch, flatness and accessibility. The centre of the 1 km transect is located at S25°55'36", E28°17'52". The ground surface along the transect is flat to within ±1 m when the mean slope (<1° upward, north to south) is removed. The terrain has a similarly gentle slope upward from east to west. The season (late autumn to early winter) was chosen for low cloud, low wind speed and minimal day-to-day variability. Solar irradiance levels were driven almost exclusively by Aerosol Optical Depth (AOD), although light cirrus cloud and early morning fog was present on occasion. Aerosols at the site are largely from biomass (grass) fires at this time of year. The site does undergo fairly large diurnal temperature fluctuations which gives rise to moderate-strong convective turbulence towards midday. The campaign was conducted between 18 June and 1 July,2013.

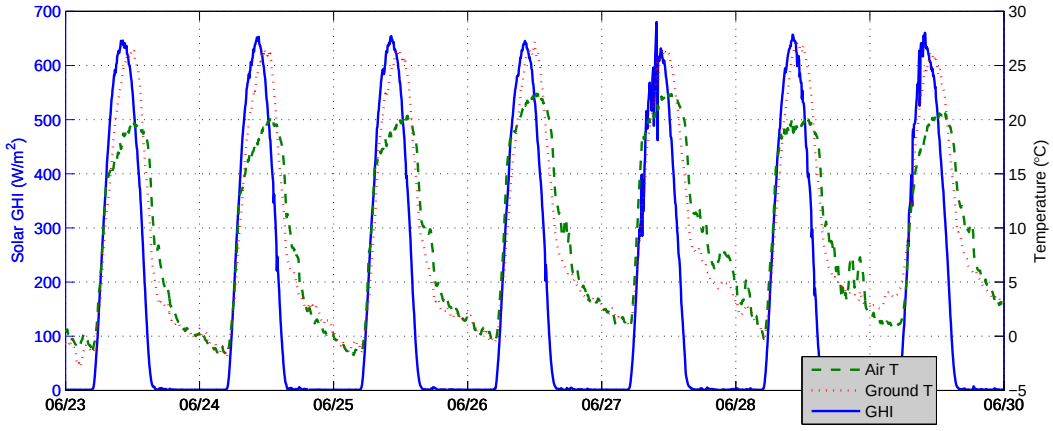

Figure 5. GHI, Air and Ground Temperature

The solar Global Horizontal Irradiance (GHI) together with ground and air temperatures for the last 7 full days of the campaign are plotted in Figure 5.

Ground and air temperature trend together with a diurnal separation as ground temperature exceeded air temperature during the middle of the day and dropping faster than air temperature in the afternoon. Sunrise over the course of the campaign was within a few minutes of 4:54 UTC, local noon likewise near 10:10 UTC and sunset near 15:25 UTC. Sub-zero temperatures were encountered after 00:00 UTC on occasion with formation of some fog, dew or frost. Winds were predominantly from the southerly direction at night and north-westerly direction during the day. The wind changeover times were about 07:00 UTC and 17:00 UTC. The wind statistics and wind run over the period 23 to 29 June, 2013 are given in Figure 6. The wind run has a characteristic diurnal sawtooth shape, but strongly dominated by the day-period westerly component. Mean night-period (17:00 to 07:00 UTC) wind speed was 1 m/s, and mean day-period (07:00 to 17:00 UTC) wind speed was 2.4 m/s. There was a treeline (visible in Figure 4) due south through to south-east of the transect, and the night-period turbulence observed between 17:00 UTC and 07:00 UTC could have been somewhat affected by the trees. However, the grassland to the north and west was free of any significant ground obstacles for at least 1500 m. Given the relatively low wind speeds, the measurements are believed to representative of the late autumn/winter season in this plateau grassland environment.

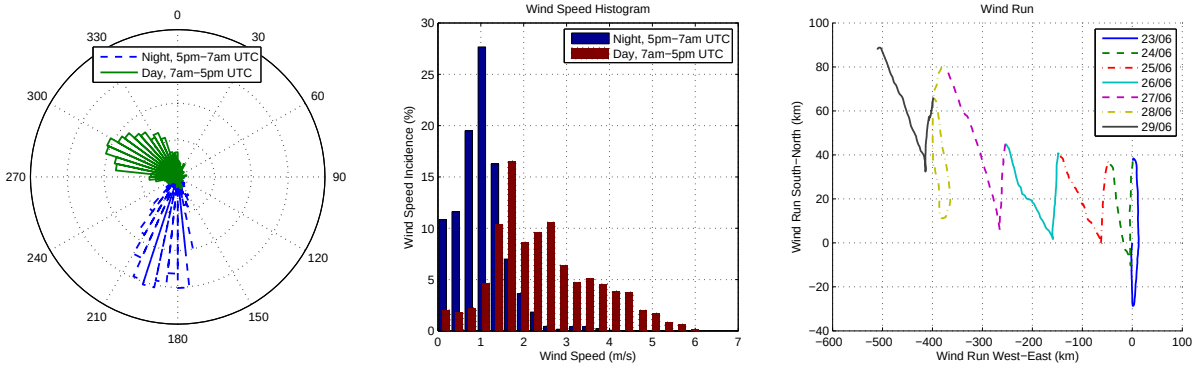

Figure 6. Wind Rose (left), Speed (centre) and Run (right)

The general spectral reflectance of the ground surface was measured in the region of the transect using an Analytical Spectral Devices (ASD) FieldSpec 3 spectroradiometer and a Spectralon® white reference tablet.

5. PRELIMINARY ANALYSIS AND RESULTS

5.1 Sonic Anemometers and SLS Scintillometer

Turbulence strength showed reasonably clear vertical stratification and decrease with height from about 6:45 to about 13:10 UTC, being from about 3.5 hours before local noon to about 3 hours after local noon. Strong dips in turbulence strength appeared to be more common at greater height during this core daytime period. Ground level (1.7 m) turbulence showed very clear, deep minima about one half hour after sunrise and about one hour before sunset. The afternoon minimum in turbulence was clearly evident at all heights, but the morning minimum was much more obvious at ground level (1.7 m) that at the heights of the sonic anemometers. There was some evidence of the minimum in turbulence lagging at greater heights by a small margin during the evening minimum but by a larger margin during the morning minimum. Turbulence stratification at night was generally more complex and chaotic, but periods of systematic vertical distribution were evident. For a period of 1 hour after sunset (until the end of nautical twilight), there was generally a particularly clear stratification with turbulence strength decreasing strongly with height. This twilight period could be of interest since light levels may still allow for long-range surveillance with sufficiently sensitive sensors. After twilight there was typically a transitional period including strong spikes in turbulence mainly at the 4.6 m and 10.2 m levels as the daytime wind dropped and the night wind began. Inverted distributions and turbulent layers at various heights became common until the morning minimum. After 19:15 UTC and before the morning minimum it was common to observe maximum turbulence at the 10 m height sonic anemometer. Strong spikes in night-time turbulence were quite frequent, particularly at the 10 m level.

Table 2. Times of Key Events and Periods

Event	Time (UTC)
Sunrise	4:54
Morning Turbulence Minimum	5:30
Wind Swing to WNW	7:00
Local Noon	10:10
Afternoon Turbulence Minimum	14:25
Sunset	15:25
Nautical Twilight End	16:20
Wind Swing to SSW	17:00

Period	Time (UTC)
Day Wind	07:00 - 17:00
Core Daytime	6:40 - 13:10
Twilight	15:15 - 16:00
Evening Transition	16:00 - 17:00
Night Wind	17:00 - 07:00
Core Nighttime	19:15 - 5:00

Values of C_n^2 derived from the SLS20 scintillometer and the sonic anemometers are plotted for two days in Figure 7. The core daytime period (3.5 hours before local noon to 3 hours after local noon), morning and evening turbulence minima as well as the twilight periods are clear.

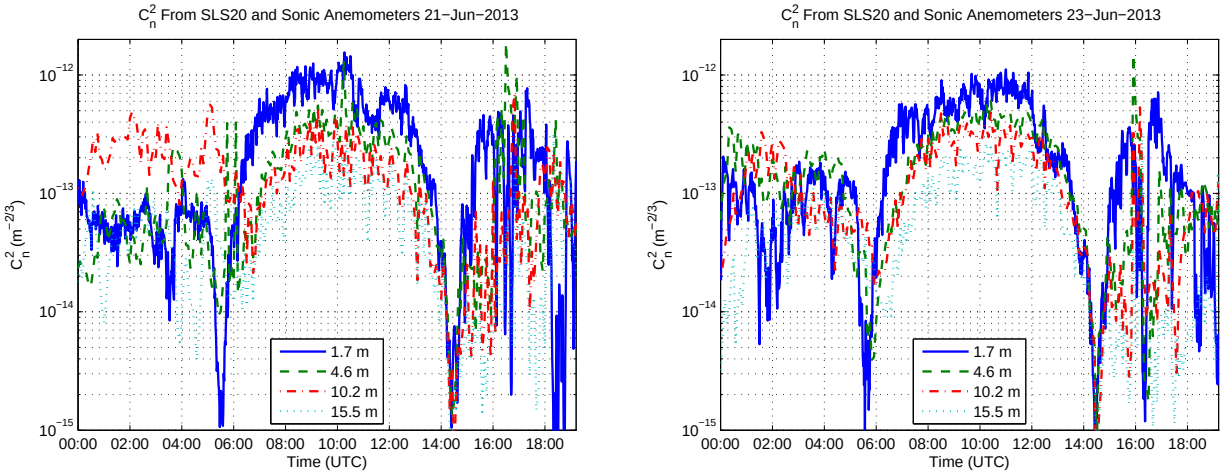

Figure 7. C_n^2 From SLS20 and Sonic Anemometers

Some of the simplest models for variation of C_n^2 with height are of the form

$$C_n^2(z) = C_n^2(z_0)z^{-k}, \tag{1}$$

where z is the height above ground, z_0 is the reference height for the anchor value of C_n^2 and k is a period-dependent parameter.

For C_n^2 derived from the sonic anemometers during the core daytime period at Rietvlei, the mean best fit log-log slope with respect to height was $k = -0.70$ with a standard deviation of 0.24.

If the data from the SLS20 scintillometer at 1.7 m height is included with the sonic anemometer data in the log-log fit, the mean best fit value of k is -0.66 with a standard deviation of 0.26. This suggests good power-law agreement between the SLS scintillometer and the sonic anemometers for the core daytime period.

5.2 Sonic Anemometers and BLS Scintillometers

A few periods were chosen in which to compare the turbulence strength derived from the BLS900 scintillometers to that derived from the sonic anemometers. This was a direct comparison without any effort to compensate the BLS results for slant path bias. Figure 8 shows some typical results.

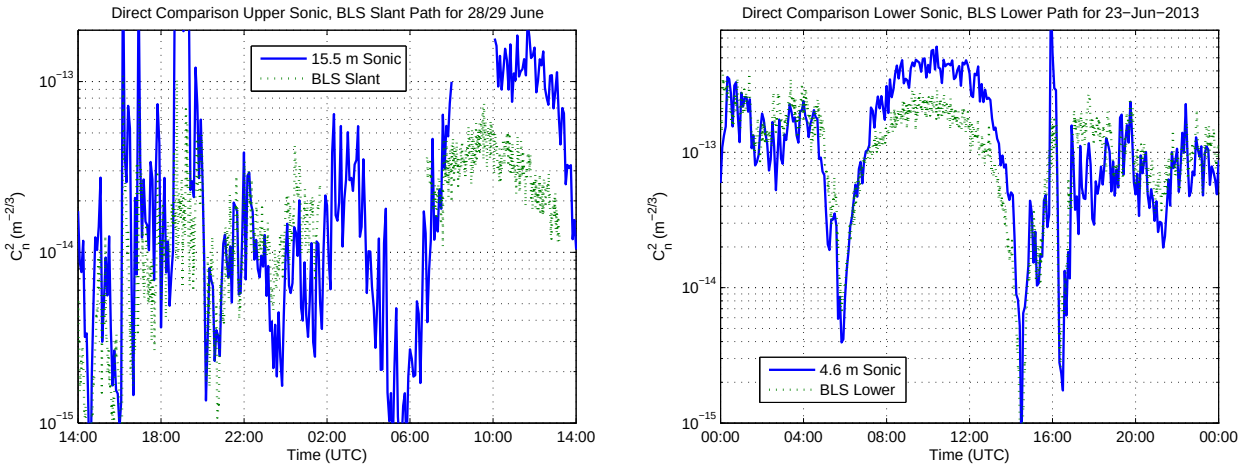

Figure 8. Direct Comparison of C_n^2 from Sonic Anemometers and BLS900 Scintillometers

The expectation was that the slant path BLS900 results would compare well to the results from the uppermost sonic anemometer (15.5 m height) since the slant path BLS900 would peak in sensitivity very near this height. Likewise, the lower sonic results were expected to track the lower BLS900 path. Figure 8 suggests that the two sets of results compare reasonably well during the night, but the absolute consistency breaks down during the core daytime convective period. This pattern for the upper sonic anemometer compared to the slant-path BLS900 and lower sonic compared to the lower BLS900 is consistent across the dataset.

A further observation was that across the whole dataset, the 5 minute averages of C_n^2 derived from the sonic anemometers showed greater variability that those from the BLS900 scintillometers. This is to be expected, since the BLS900 integrates over a much greater volume of air. While the values of C_n^2 derived from the sonic anemometers and the BLS scintillometers did not always agree very well in absolute terms, there was a very obvious and expected tendency of the slant path BLS900 results to co-vary with the upper and (to a lesser degree) mid-level sonic anemometers rather than the low-level sonic anemometer.

6. CONCLUSIONS

The 2013 field campaign at Rietvlei Nature Reserve to measure the vertical profile of atmospheric turbulence strength has been described in relation to operation of optical imaging systems near ground level. A number of measurement techniques including scintillometry, sonic anemometry and high speed videography of point sources were used.

The daytime vertical distribution of turbulence was largely systematic and driven by the convective process as expected. Vertical distribution of turbulence strength at night was more complex and chaotic and perhaps driven in part by intermittent katabatic airflow in the presence of stable layer formation at ground level. Discrete layers and strong spikes in turbulence strength at night are thought to result from wind-driven mixing of air layers of different temperatures.

Most existing models of vertical variation of turbulence strength are large scale models of the electro-optical community disregarding the special features of the atmospheric surface layer such as the strong variability of atmospheric stability driven by the heating and cooling from the ground. There are some meteorological models based on the Monin-Obukhov similarity theory which parametrise the height dependency of turbulence with the atmospheric stability based on the Obukhov-length. This campaign shows that there is small scale but potentially predictable detail in the turbulence strength picture within the lower atmospheric boundary layer. Combining different methods of turbulence measurement can contribute to understanding of the nature and origin of these details.

The dataset recorded at Rietvlei, particularly the video dataset requires further and deeper analysis and is a promising source of further insight.

7. ACKNOWLEDGMENTS

We thank the German Federal Armed forces Technical Center (WTD91) for their financial support of this campaign in the frame of the ATLIMIS-project. Additional funding was provided by Armscor. The management of Rietvlei Nature Reserve is thankfully acknowledged for granting permission to use this area in the reserve. We also thank Master Towers for low-impact, timeous installation and removal of the 30 m lattice mast. Fire warning services for the Rietvlei campaign were provided by the Advanced Fire Information System (AFIS[8]).

REFERENCES

[1] Weiss-Wrana, K. and Balfour, L. S., "Statistical analysis of measurements of atmospheric turbulence in different climates," *Optics in Atmospheric Propagation and Adaptive Systems IV* **4538**(1), 93–101, SPIE (2002).

[2] Weiss-Wrana, K. R., "Turbulence statistics in littoral area," *Optics in Atmospheric Propagation and Adaptive Systems IX* **6364**(1), 63640F, SPIE (2006).

[3] Sprung, D., Grossmann, P., Sucher, E., Weiss-Wrana, K., and Stein, K., "Stability and height dependant variations of the structure function parameters in the lower atmospheric boundary layer investigated from measurements of the long-term experiment verturm (vertical turbulence measurements)," *Optics in Atmospheric Propagation and Adaptive Systems XIV* **8178**(1), 817809, SPIE (2011). http://link.aip.org/link/?PSI/8178/817809/1.

[4] Vernin, J., "SCIDAR measurements and model forecasting of free atmosphere turbulence.," in [*European Southern Observatory Conference and Workshop Proceedings*], D'Odorico, S. and Swings, J.-P., eds., *European Southern Observatory Conference and Workshop Proceedings* **24**, 279–288 (1986).

[5] Wilson, R. W., "SLODAR: measuring optical turbulence altitude with a Shack-Hartmann wavefront sensor," *Mon. Not. R. Astron. Soc.* **337**, 103–108 (Nov. 2002).

[6] Zilberman, A. and Kopeika, N. S., "Lidar measurements of atmospheric turbulence vertical profiles," *Free-Space Laser Communication Technologies XVI* **5338**(1), 288–297, SPIE (2004).

[7] Scintec, *Scintec Boundary Layer Scintillometer User Manual* (2008). www.scintec.com.

[8] Frost, P. and Annegarn, H., "Providing satellite-based early warnings of fires to reduce fire flashovers on south africas transmission lines," in [*Geoscience and Remote Sensing Symposium, 2007. IGARSS 2007. IEEE International*], 2443–2446 (2007).